Eng. Sci., 2022, **18**, 299–307

Engineered Science

DOI: https://dx.doi.org/10.30919/es8d603

Cyclodextrin Modified Graphene Membrane for Highly Selective Adsorption of Organic Dyes and Copper (II) Ions

Mengmeng Cheng,[1] Chenxue Yao,[1] Yan Su,[1] Jinglei Liu,[1] Lijian Xu,[1] Jidong Bu,[1] Hua Wang[2,*] and Shifeng Hou[1,*]

Abstract

Organic dyes and copper ions are the main industrial wastewater pollutants, which have potential threats to the environment and humans. Here, a novel β-cyclodextrin decorated reduced graphene oxide complex (rGO-β-CD) is synthesized by wet-chemical strategy. The characterization results confirm the successful synthesis of the rGO-β-CD complex, which also exhibits high stability in the polar solvent. In addition, the quantitative analysis reveals that rGO has excellent loading capacity for β-CD (up to 19 wt.%). Benefiting from the tightly stacked structure, the rejection rate of the rGO-β-CD membrane for rhodamine B (RhB), methyl orange (MO), and even blue (EB) is nearly 100%. Furthermore, the membrane displays significantly lower copper ions permeation in mixed ion solutions, with a permeability of 0.05 mmol m^{-2} h^{-1}. Importantly, the membrane exhibits specific adsorption for copper ions, resulting in a Zn^{2+}/Cu^{2+} selectivity of 4.6. Based on the results, the rGO-β-CD membrane was observed to be a promising material for wastewater treatment. This study provides a novel rGO-β-CD membrane to separate organic dyes and copper ions from wastewater.

Keywords: Graphene; Cyclodextrin; Membrane; Ions removal; Water treatment.
Received: 31 May 2021; Revised: 19 July 2021; Accepted: 14 August 2021.
Article type: Research article.

1. Introduction

Organic dyes and heavy metal ions are the main pollutants in industrial wastewater. Some organic dyes and heavy metals are not only non-biodegradable but also difficult to be discharged through metabolism, potentially causing serious health hazards to humans and other organisms.[1] Untreated organic dyes discharged into water will cause eutrophication of the water body, which could damage the animal and plant communities seriously in water. Moreover, excessive copper ions can lead to toxic effects such as serious mucous membrane stimulation and corrosion, liver and kidney damage, extensive capillary damage, and even liver and kidney necrosis.[2,3] Therefore, toxic copper ions in industrial wastewater must be effectively removed before releasing them into the environment.

Generally, the methods of ion removal include coagulation, adsorption, chemical precipitation, ion exchange, reverse osmosis, and membrane separation.[4-6] Among these available technologies, adsorption is the most widespread technology due to its simplicity, flexibility, and economy. Recently, β-cyclodextrin (β-CD) has received much attention in wastewater treatment due to its special cavity structure tends to combine with metal ions or organics to form clathrate through the host-guest effect.[7] However, the recovery of β-CD in water is difficult due to the lack of a suitable platform to achieve high-efficiency loading of β-CD.

Fortunately, graphene materials are expected to become efficient carriers owing to the large surface area, sufficient active sites, and easily modified characteristics.[8,9] Moreover, graphene materials have been reported to be used in water treatment[10] as well as gas and ion separation[11,12] due to their excellent film-forming and ion-sieving properties.[13] Here, a novel multilayer membrane based on the β-cyclodextrin modified partially reduced graphene oxide (rGO-β-CD) is presented to remove Cu (II) ions from wastewater. The membrane can not only completely block the organic dyes in the solution but also specifically remove the copper ions in simulated wastewater. This paper provides a new adsorptive membrane system for the removal of organic dyes and copper ions and proposes a synergistic strategy for efficient

[1] *School of Chemistry and Chemical Engineering, National Engineering Research Center for Colloidal Materials, Shandong University, Jinan, 250100, China.*
[2] *School of Public Health, Jining Medical University, Jining, 272013, China.*
**E-mail:* shifenghou@sdu.edu.cn (S. Hou);
wanghua@mail.jnmc.edu.cn (H. Wang)

wastewater treatment.

2. Experimental section

2.1 Chemicals and materials

Graphite powder was provided by Shandong Leadernano Technology Co., Ltd. β-cyclodextrin (β-CD), Evans blue (EB), methyl orange (MO) and rhodamine B (RhB), hydrochloric acid (HCl), hydrazine hydrate ($N_2H_4 \cdot H_2O$), potassium chloride (KCl), sodium chloride (NaCl), calcium chloride ($CaCl_2$), copper chloride ($CuCl_2$), cobalt chloride ($CoCl_2$), nickel chloride ($NiCl_2$) and zinc chloride ($ZnCl_2$) were bought from Shanghai Macklin Biochemical Co., Ltd. All the raw materials and chemical reagents used in the synthesis process were of analytical grade without any further purification.

2.2 Synthesis of rGO and rGO-β-CD complex

The preparation approach of the complex and membrane is exhibited in Fig. 1. GO powder was synthesized by the modified Hummers' method.[14] Then the rGO-β-CD complex was prepared as follows: First, the mixed solution of GO (0.5 mg/mL, 20.0 mL) and β-CD (4 mg/mL, 20.0 mL) was obtained by stirring at room temperature. Then add a certain proportion of hydrazine hydrate solution and ammonia water solution. Finally, the rGO-β-CD was collected by stirring in a water bath at 45 °C for 5 hours. A similar approach was adopted to prepare rGO, except that β-CD was not added during the preparation process.

2.3 Preparation of the membranes

The membrane was prepared by a vacuum filtration method at 1 bar transmembrane pressure. Next, 0.5 mL of rGO-β-CD solution was vacuum filtered through a polyvinylidene fluoride (PVDF) membrane to produce the rGO-β-CD membrane. Similarly, 0.5 mL rGO aqueous solution was used to prepare the rGO membrane. At last, the obtained products were vacuum dried under mild conditions at 35°C.

2.4 Characterization

Transmission electron microscope (TEM) and Scanning electron microscope (SEM)) were applied to detect the surface structure of the complex and membrane. X-ray diffraction (XRD) patterns were investigated with DMAXRB-III. The molecular structures of rGO and rGO-β-CD were analyzed using Fourier transform infrared spectrometer (FT-IR, MAGNA-IR 550) and an Ultraviolet visible spectrophotometer (UV-vis). The content of each component in the rGO-β-CD complex was analyzed by a thermogravimetric analyzer (TGA) heated from room temperature to 790 °C in a nitrogen atmosphere. The concentration of ions was determined using inductively coupled plasma mass spectrometry (Agilent 7800 ICP-MS).

3. Results and discussion

3.1. Characterization of rGO-β-CD membrane

According to Fig. S2, the rGO-β-CD complex aqueous solution prepared by chemical reduction can maintain uniformity within 24 hours, which is an attribute to the stability and water solubility of β-CD.[15,16] Then the rGO-β-CD membrane is uniformly deposited on a polytetrafluoroethylene (PTFE) substrate by vacuum filtration,[17,18] and a freestanding rGO-β-CD membrane is obtained after peeling off (Fig. 2a). The TEM image of the rGO-β-CD complex shows that β-CD has been successfully loaded on the surface of rGO (Fig. S3). As we can see in Fig. 2, the filtration of rGO-β-CD dispersion through a membrane filter yielded a flexible membrane (d = 15 mm). In addition, typical wavy wrinkles are formed on the rGO-β-CD membrane, which provides special channels for small molecules and ions (Fig. 2b). As shown in Fig. 2c, the cross-sectional view of rGO-β-CD membrane indicates its well-packed layered structures. This is because rGO-β-CD sheets can be assembled into a multilayer macrostructure under vacuum filtration-induced directional flow. Moreover, the thickness of the membrane is 310 nm, and it is a multilayered structure membrane. Fig. S4 exhibits a diffraction peak value of 26.5° for rGO nanosheets, and after grafting with β-CD, rGO-β-CD shows a diffraction peak value at 24.78°, indicating the interlayer spacing is slightly expanded.[19] All of these indicate that GO was successfully reduced and modified. Moreover, rGO-β-CD maintains a similar stacking structure to rGO.

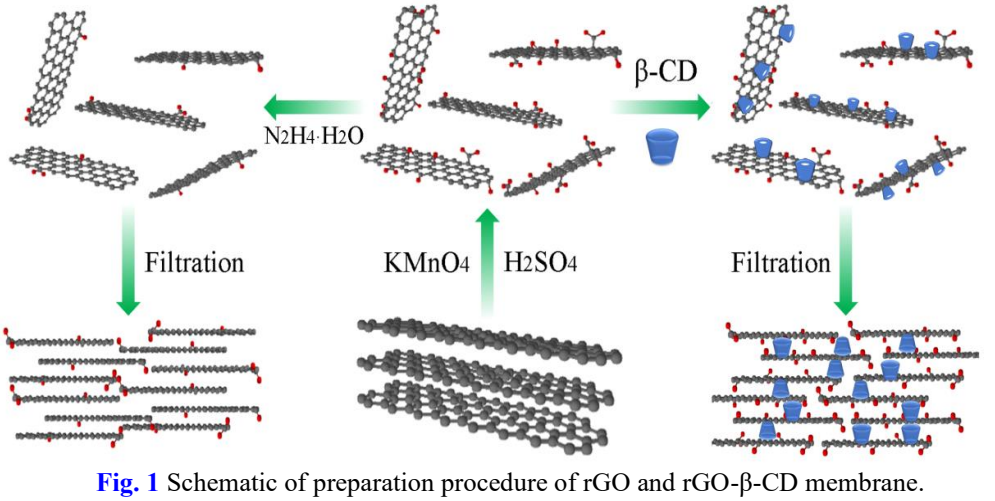

Fig. 1 Schematic of preparation procedure of rGO and rGO-β-CD membrane.

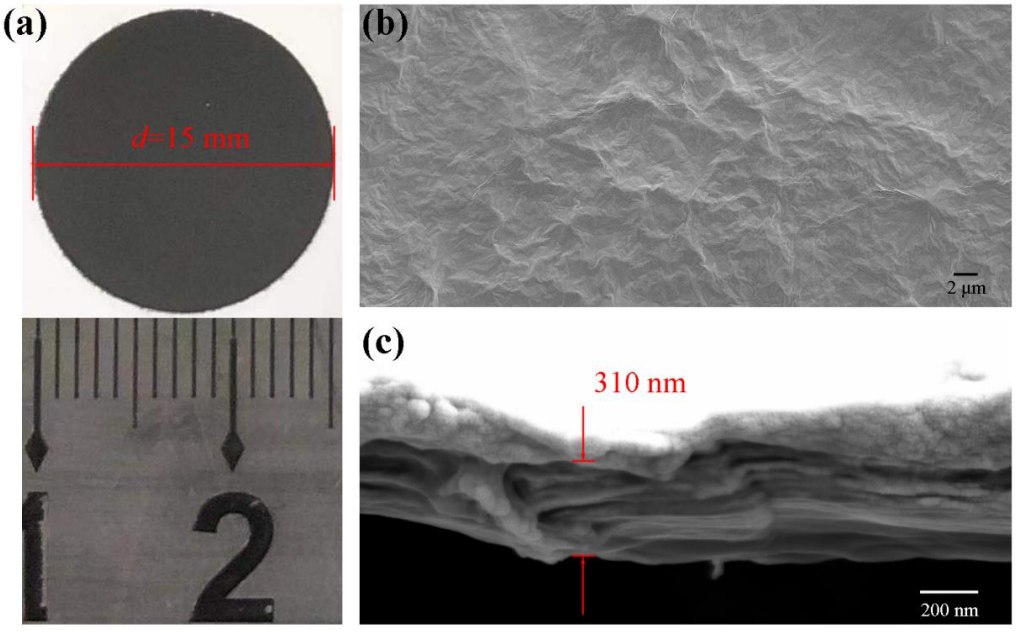

Fig. 2 (a) Digital photo of rGO-β-CD membrane on PTFE substrate. (b) Surface and (c) cross-section SEM images of the rGO-β-CD membrane.

The functionalization of the rGO-β-CD complex is further confirmed by FT-IR and UV-vis studies. The FT-IR spectra in Fig. 3a and Table S1 show that the rGO-β-CD complex contains the vibrational bands of β-CD at 1029 cm^{-1} (coupling vibration of −C−C and −C−O), 1159 cm^{-1} (stretching vibration of −C−O−C) and 2926 cm^{-1} (stretching vibration of $-CH_3$ and $-CH_2$).[20,21] Similarly, a vibration band of rGO is observed for rGO-β-CD at 1638 cm^{-1}, which should be due to the C=C vibration. The FT-IR results indicate that the rGO surface was successfully combined with β-CD molecules. In Fig. 3b, UV-vis spectroscopy shows that GO displays a maximum absorption at 210 nm, which may be caused by the π-π* transition. Besides, the adsorption peak at 300 nm is related to the n-π* transition of the lone pair electron on the carbonyl group.[22] After modification, the absorption peak at 210 nm is red-shifted to 265 nm, which suggested that the electronic conjugation was restored during the reduction process.[23]

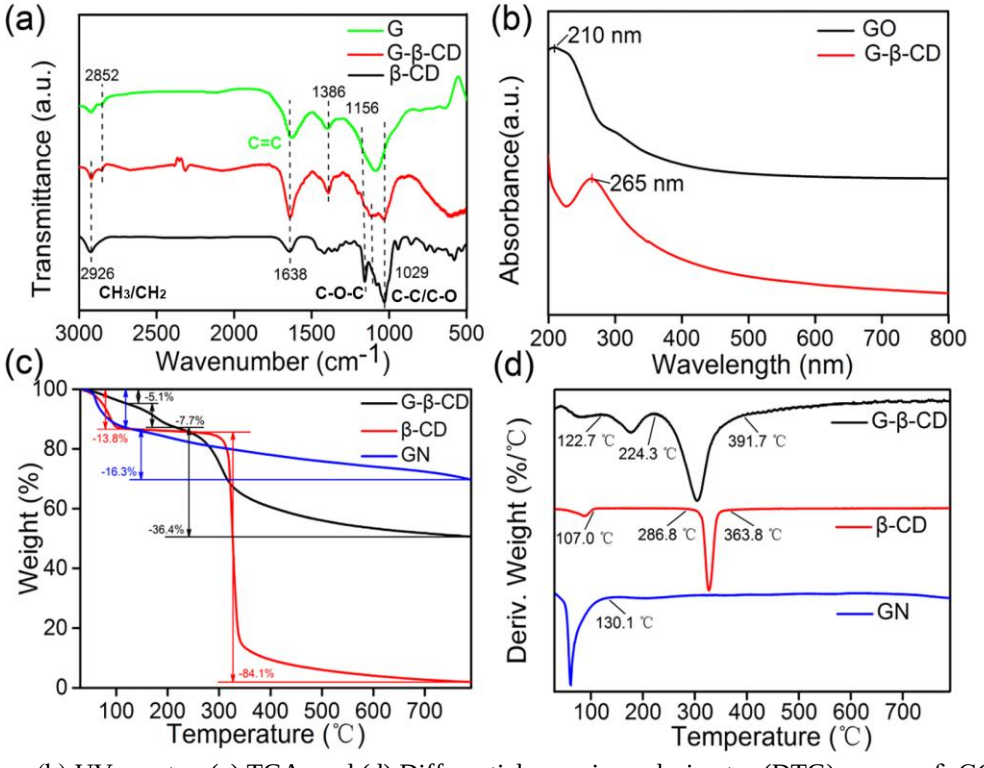

Fig. 3 (a) FT-IR spectra, (b) UV spectra, (c) TGA, and (d) Differential scanning calorimetry (DTG) curves of rGO before and after functionalization with β-CD.

The degree of functionalization is estimated by TGA. As shown in Fig. 3c, the TGA curve of rGO-β-CD shows a slight loss stage below 100 °C (5.1 wt.%) owing to the evaporation of moisture. When the temperature reached 220−400 °C, rGO-β-CD showed a significant weight loss stage (36.4 wt.%) due to the thermal decomposition of β-CD and oxygen-containing groups on rGO. However, rGO-β-CD shows ~19 wt.% extra weight loss at the end of 790 °C as compared to rGO, which is attributed to the loading of β-CD. Fig. 4a shows that in the X-ray photoelectron spectroscopy (XPS), the ratio of C to O is ~3.2:1. The C 1s spectra of GO (Fig. 4c) and rGO-β-CD (Fig. 4b) both exhibit four typical peaks.[24,25] However, according to the changes in peak area corresponding to the four types of carbon bonds (Fig. 4d), the proportion of C-C/C=C bonds in rGO-β-CD increases greatly from 40.55% to 54.07%. Meanwhile, the relative contents of C-O, C=O, and O-C=O reduced from 35.12%, 15.15%, and 9.18% to 32.26%, 8.58%, and 5.09%, indicating the chemical reduction leads to the disappearance of some oxygen groups.[26,27]

3.2. Removal of organic dyes by rGO-β-CD membrane

Encouraged by the successful modification of β-CD on the rGO surface, the separation performance for organic dyes is investigated, including Evans blue (EB), methyl orange (MO), and rhodamine B (RhB). The structures of typical dye molecules used for the permeation experiments are exhibited in Fig. S5. The concentration of all feed solutions was 0.1 mM, and the permeate solutions are collected at 24, 48, 72, and 96 hours, respectively. As presented in Fig. 5, the absorption peaks of the dye molecules in the permeated solution have disappeared. Moreover, the absorption spectra of permeate solution almost overlap at different time points, which indicates that organic dyes such as EB, MO, and RhB can hardly pass through the rGO-β-CD membrane. In Fig. 5d, the permeation rates of EB, MO, and RhB molecules are calculated in 96 h, which were 0.31×10^{-4}, 1.58×10^{-4}, and 0.70×10^{-4} mmol m^{-2} h^{-1}, respectively. The permeation rates demonstrate that almost all organic dyes have been successfully retained by the rGO-β-CD membrane and the difference in permeation rate was related to the size of dye molecules. According to the structure of the rGO-β-CD membrane, this could be ascribed to the synergy of multi-mechanism: (1) absorption caused by π-π interaction between organic dyes and benzene ring in graphene; (2) formation of inclusion complex owing to the interaction between organic dyes and β-CD molecules; (3) physical sieving mechanism controlled by the interlayer spacing of rGO-β-CD membrane.[28-30]

3.3. Removal of Cu (II) ions from mixed ionic solution

To verify the separation performance of copper ions, a mixture solution with K^+, Na^+, Ca^{2+}, and Cu^{2+} has been employed as a feed solution. Over time, the changes in ion permeation measured for the permeate solution shows a similar trend. Ion permeation increases significantly in the beginning and then gradually stabilized over time as shown in Fig. 6. This phenomenon may be attributed to the existence of hydrophobic nanochannels between the interlayers of the rGO-β-CD membrane in the initial stage. When the nanochannels are large enough, hydrated ions can enter the permeate side from the feed side. However, the variations in the amplitudes of ion permeation decreases gradually (Fig. 6f)

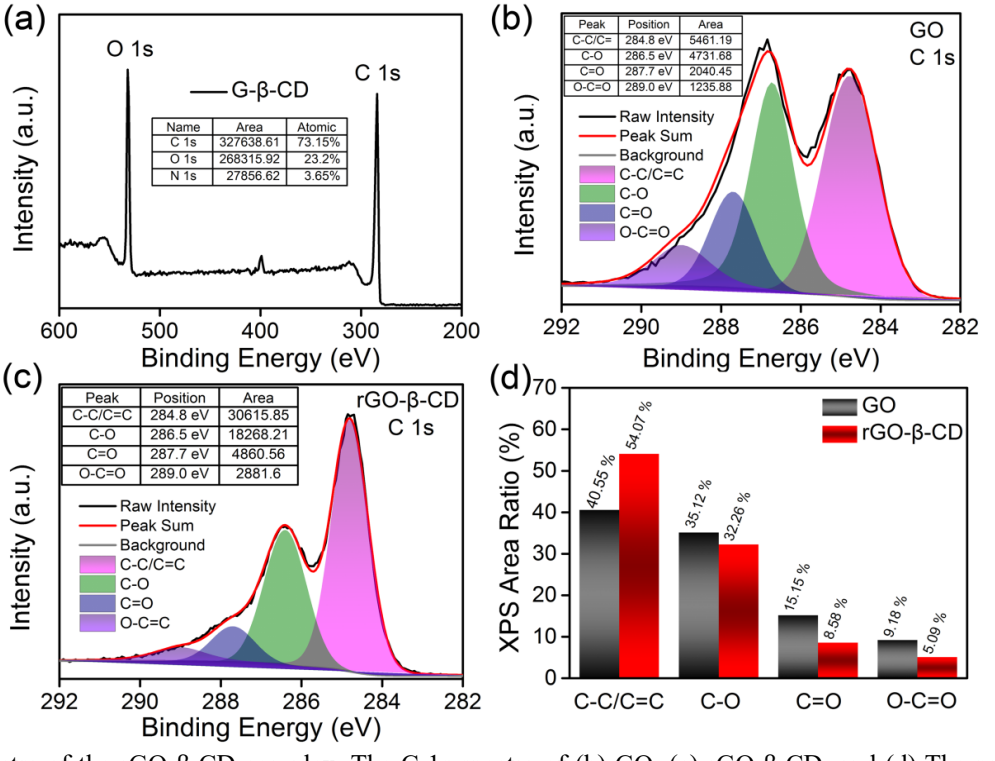

Fig. 4 (a) XPS spectra of the rGO-β-CD complex. The C 1s spectra of (b) GO, (c) rGO-β-CD, and (d) The proportion of carbon bonds in GO and rGO-β-CD complex.

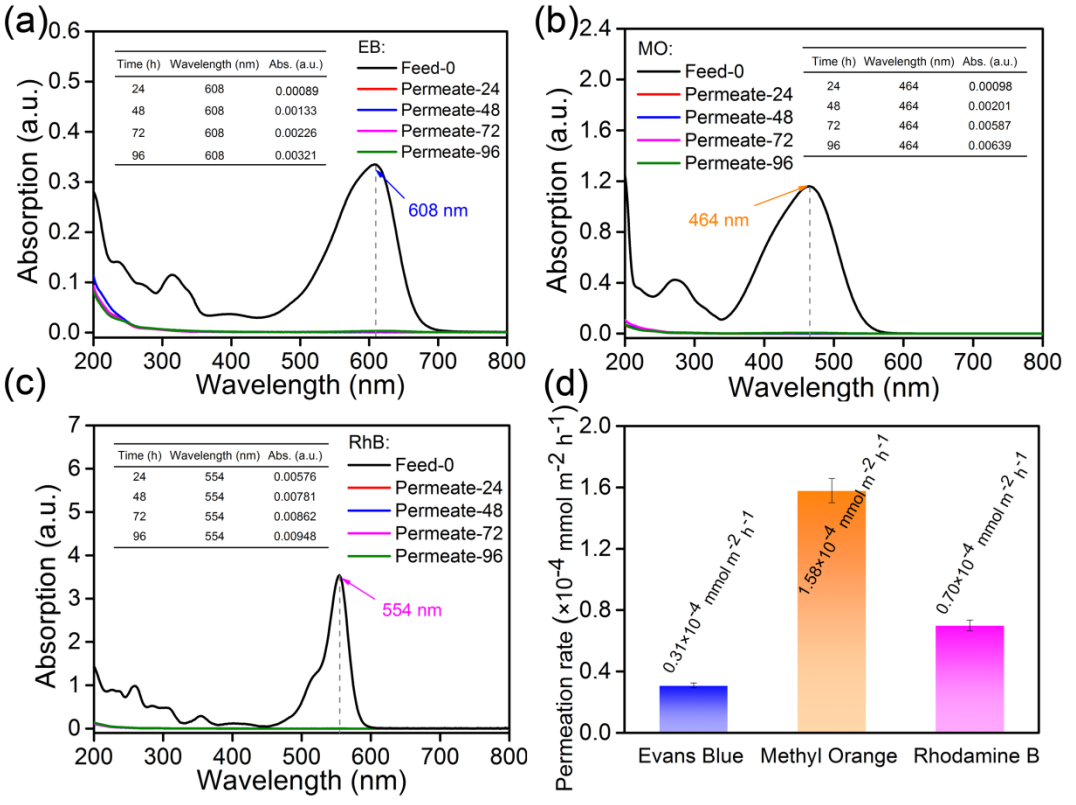

Fig. 5 The UV-Vis absorption spectra of (a) EB, (b) MO, (c) RhB, and (d) the permeation rate of organic dye molecules.

due to the coordination between Cu (II) ions and oxygen-containing groups in rGO. Meanwhile, the accumulation of Cu (II) ions between the layers lead to a reduction in the size of the nanochannel, which blocked the permeation through the physical ion-sieving mechanism. Moreover, the order of ion concentration in permeate solution is $K^+ > Na^+ > Ca^{2+} > Cu^{2+}$ (Fig. 6e), suggesting that the rGO-β-CD membrane has ion-sieving performance.[31,32] When the size of metal ions is larger than that of nanochannels, the metal ions are blocked on the feed side. Hence, the order of ion concentration is related to the hydrated ionic diameter, with the hydrated ionic diameter (d_H) being in the following order (Table S2): K^+ (6.62 Å) < Na^+ (7.16 Å) < Ca^{2+} (8.24 Å) < Cu^{2+} (8.38 Å). Moreover, the dehydrated ion is smaller than the cavity of β-CD, which can form clathrate through host-guest interaction, especially when the dehydrated ionic diameter (d_D) highly matched the size of the inner cavity. Generally, the characterizations prove that the rGO-β-CD membrane can efficiently separate Cu (II) ions from the mixed ionic solution by multiple mechanisms.

To verify the effect of β-CD on Cu (II) ions separation efficiency, we have measured the permeation of mixed ionic solution by rGO membrane without β-CD modification. As shown in Fig. 7a, the ion concentration in the rGO membrane exhibits similar trends as that of those in the rGO-β-CD

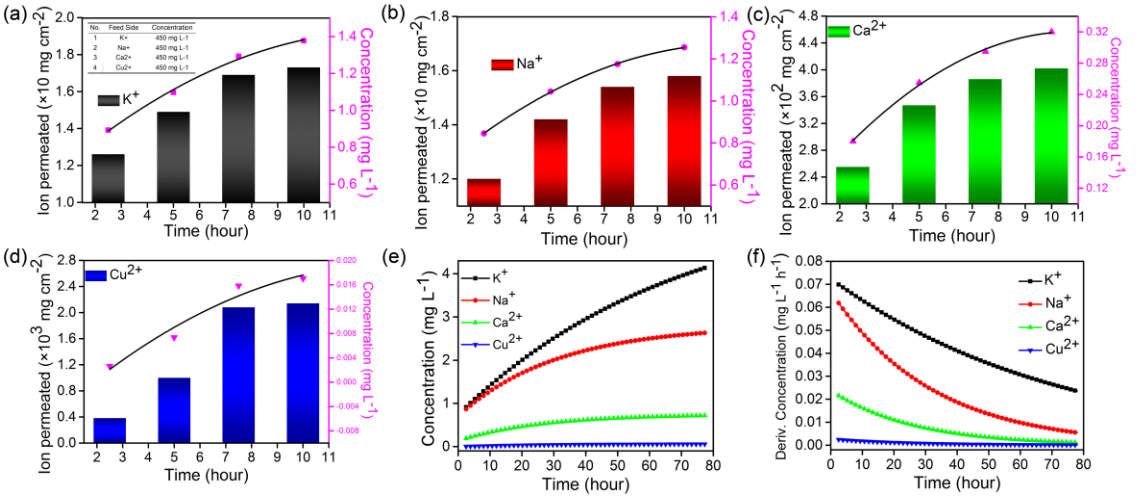

Fig. 6 The permeation parameters of the rGO-β-CD membrane to (a) K^+, (b) Na^+, (c) Ca^{2+}, (d) Cu^{2+}; and the comparison of (e) concentration and (f) permeation amplitude.

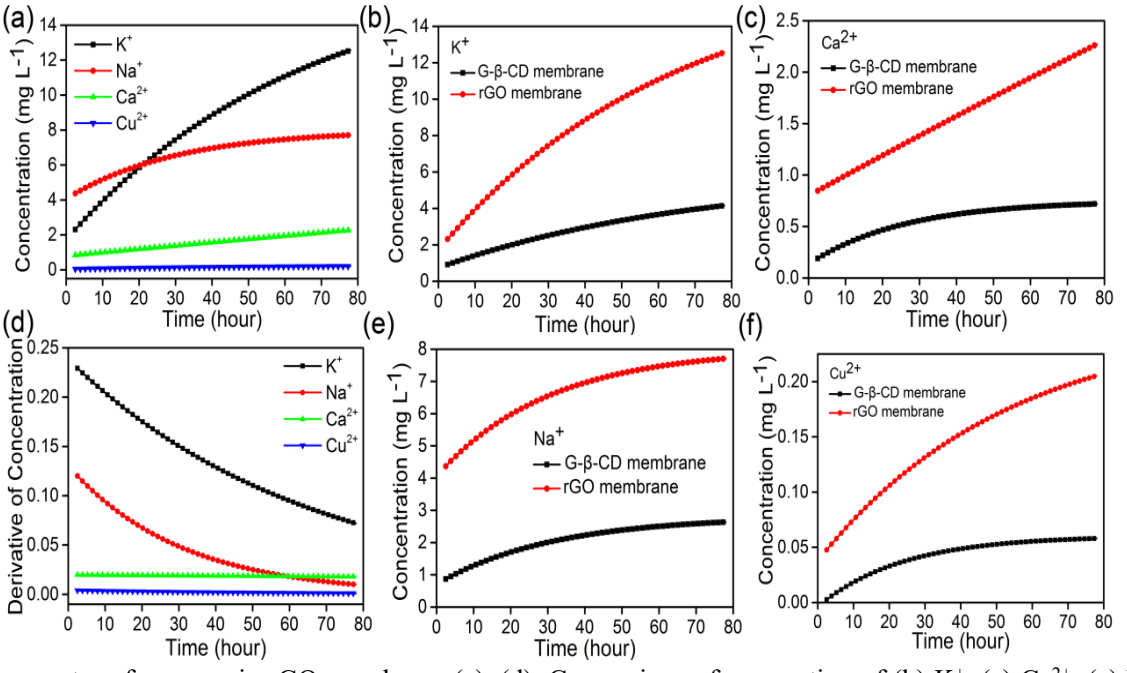

Fig. 7 Ion transport performance in rGO membrane (a), (d). Comparison of permeation of (b) K^+, (c) Ca^{2+}, (e) Na^+, and (f) Cu^{2+} ions between rGO and rGO-β-CD membrane.

membrane, indicating that both coordination and physical ion-sieving mechanisms exist in this process. Nevertheless, when compared with the rGO-β-CD membrane quantitatively, the ion concentrations in permeate solution are obviously increased (Figs. 7 b, c, e, f) due to the absence of β-CD, which can form complex with cations. In general, the β-CD functionalized membrane has higher separation efficiency than the rGO membrane in metal ions removal.

To further evaluate the specificity of rGO-β-CD membrane for Cu (II) ions removal, a mixed ionic solution including four ions (Co^{2+}, Ni^{2+}, Cu^{2+}, Zn^{2+}) with similar hydration diameters (Table S3) has been selected to measure the permeability of ions in the rGO-β-CD membrane (Fig. 8a). Compared with the former mixed ionic solution, the ion concentration changes slightly at the initial stage due to the rGO-β-CD membrane having a wetting process where the increase of interlayer distance led to the expansion of nanochannels. In the next two stages, the ion concentration shows the same tendencies. Meanwhile, the calculated permeation rates of rGO-β-CD membrane to Co^{2+}, Ni^{2+}, Cu^{2+} and Zn^{2+} are 0.13, 0.14, 0.05 and 0.23 mmol m^{-2} h^{-1}, respectively. The selectivity ratios of Co^{2+}/Cu^{2+}, Ni^{2+}/Cu^{2+}, and Zn^{2+}/Cu^{2+} were 2.6, 2.8, and 4.6, respectively. It is noteworthy that although Co^{2+}, Ni^{2+}, Cu^{2+}, and Zn^{2+} have similar hydration diameters, the transportation of rGO-β-CD membrane to Cu^{2+} is apparently lower than other metal ions. This demonstrates that even if the ion size is uniform, the rGO-β-CD membrane is specific for Cu^{2+}. In addition, different types of Cu (II) ions removal membranes are also compared in Table S4, and as a result, the retention of rGO-β-CD membrane for Cu (II) ions is higher than that of others. Theoretically, the host-guest and sieving effects of rGO-β-CD membrane for ion removal mainly depend on the size of the ion hydration diameter and dehydration diameter. However, the tight square-planar coordination of Cu (II) ions with oxygen groups on rGO-β-CD lead to the enrichment of Cu (II) ions on the membrane.

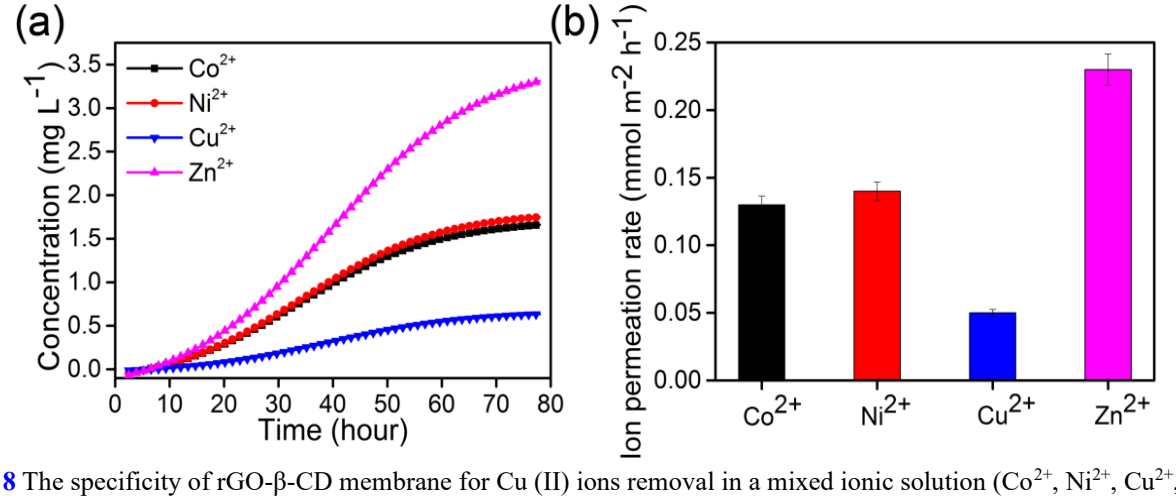

Fig. 8 The specificity of rGO-β-CD membrane for Cu (II) ions removal in a mixed ionic solution (Co^{2+}, Ni^{2+}, Cu^{2+}, Zn^{2+}).

3.4. Adsorption kinetics and isotherm

The amount of Cu (II) ions adsorbed by the rGO-β-CD complex increases rapidly in the early stage of the adsorption process (Fig. 9a). For the sake of further investigating the mechanism, pseudo-first-order and pseudo-second-order models are selected to study the adsorption kinetics in detail:

$$\log(q_e - q_t) = \log q_e - \frac{k_1 t}{2.303} \quad (1)$$

$$\frac{t}{q_t} = \frac{1}{k_2 q_e^2} + \frac{t}{q_e} \quad (2)$$

where q_e is the adsorption capacity calculated using two models; q_t is the amount of Cu (II) ions adsorbed by the rGO-β-CD complex at time t; k_1 and k_2 represent the rate constants in the two kinetic models, respectively.

The kinetic curves are obtained by nonlinear fitting using two adsorption kinetic models, as shown in Figs. 9b and c and the results are summarized in Table 1. The determination coefficients (R^2) of the pseudo-first-order model (Fig. 9b) were 0.977 and 0.891, respectively, which are lower than those of the pseudo-second-order model in Fig. 9c (0.990 and 0.998). More importantly, the q_e calculated by the pseudo-second-order model is basically equivalent to the results of the adsorption experiment. The result indicates that the Cu (II) adsorption process is more inclined to the chemical adsorption kinetic.

Table 1. Kinetic parameters of Cu (II) adsorption onto rGO-β-CD.

C_0	Pseudo-first-order			Pseudo-second-order		
mg L^{-1}	k_1 min^{-1}	q_e mg g^{-1}	R^2	k_2 g mg^{-1} min^{-1}	q_e mg g^{-1}	R^2
1	0.026	0.240	0.977	0.093	0.242	0.990
2	0.025	0.647	0.891	0.066	0.686	0.998

When the adsorption process reaches equilibrium, the distribution of copper ions in the liquid and solid states was characterized by adsorption isotherms. The adsorption isotherm has been exhibited in Fig. 9d, determined by the Langmuir model and Freundlich model, which can be described as:

$$q_e = \frac{K_L q_{max} C_e}{K_L C_e + 1} \quad (3)$$

$$q_e = K_F C_e^{1/n} \quad (4)$$

where K_L and q_{max} refer to the constant in the Langmuir model and the maximum adsorption capacity respectively; K_F and n represent the constant and heterogeneity factor in the Freundlich model.

Table 2. The isotherm parameters of Cu (II) adsorption onto rGO-β-CD.

T	Langmuir model			Freundlich model		
°C	q_{max} mg g^{-1}	K_L L mg^{-1}	R^2	n	K_F	R^2
25	35.682	0.078	0.971	3.844	8.119	0.774

The calculated results of the Langmuir and Freundlich adsorption isotherms are listed in Table 2. According to the R^2 values, the adsorption behavior of Cu (II) is more in line with the Langmuir isotherm. And it can be seen from Fig. 9d that the Langmuir model is more consistent with the experimental data than the Freundlich model. All these analyses show that the adsorption of Cu (II) by rGO-β-CD is mainly monolayer adsorption, and the adsorption active sites are evenly distributed.

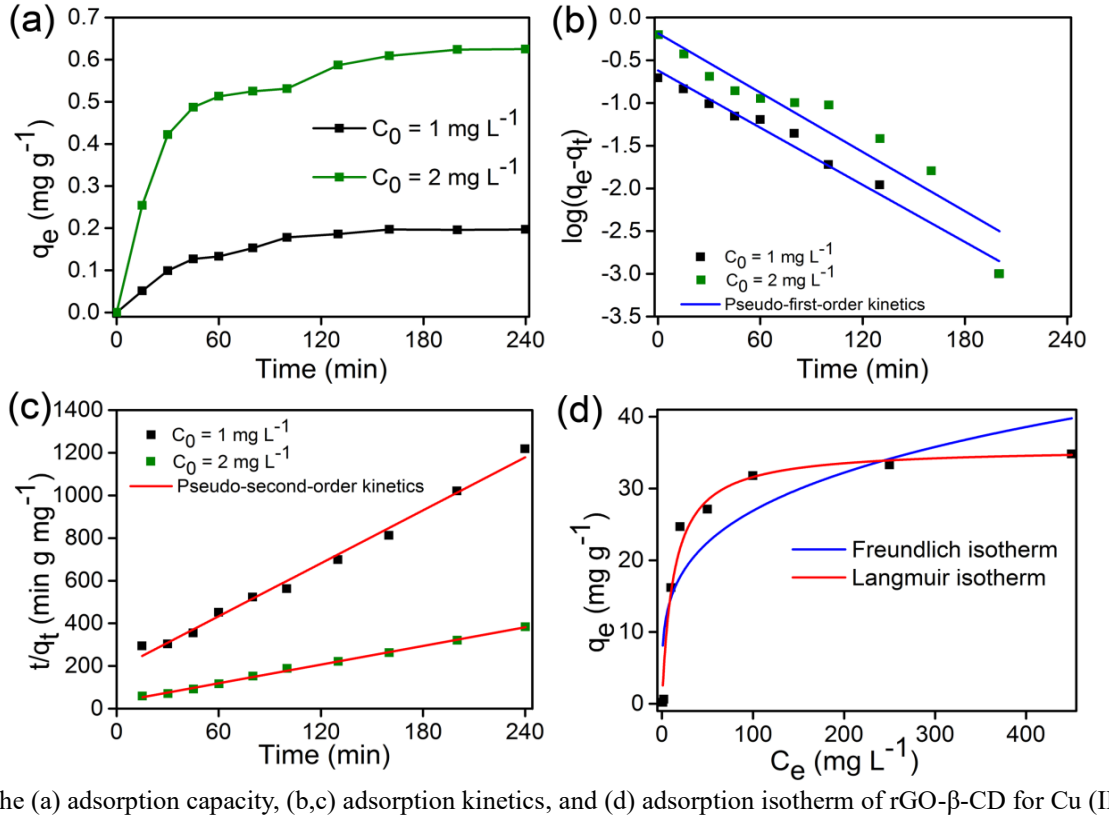

Fig. 9 The (a) adsorption capacity, (b,c) adsorption kinetics, and (d) adsorption isotherm of rGO-β-CD for Cu (II) ions.

3.5. Mechanism of Cu (II) ions removal

Based on the discussion on its characterization and Cu (II) ions removal, the unique structure of the rGO-β-CD membrane contributes to the specific removal of Cu (II) ions through multiple mechanisms, as shown in Fig. 10. Generally, Cu (II) ions can be connected to the carbonyl group by forming coordination bond, which is due to the existence of lone pair electrons.[33] Hence, square-planar coordination interaction exists between Cu (II) ions and oxygen-containing groups (*e.g.* carbonyl and carboxyl) on the surface of the membrane. Meanwhile, the hollows of β-CD tend to specifically select Cu (II) ions in mixed ionic solutions through the host-guest effect to form inclusion compounds. In addition to the above interactions, nanochannels exist between the interlayer of the rGO-β-CD membrane, and Cu (II) ions are blocked when the nanochannel is smaller than Cu (II) ions, which is also called the physical ion-sieving mechanism. Because of the combined effect of the various components in the membrane system, the rGO-β-CD membrane has a remarkable removal efficiency on transition metal ions (such as Cu^{2+}, Co^{2+}, and Ni^{2+}), especially for Cu (II) ions.

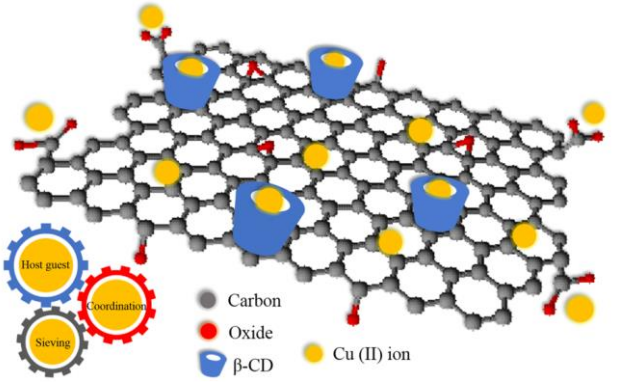

Fig. 10 The proposed multi-mechanism of rGO-β-CD membrane for the removal of Cu (II) ions.

4. Conclusions

The β-cyclodextrin functionalized multilayer structured graphene membrane has been successfully prepared by an environmentally friendly method. The TGA and XPS analysis confirm the content of β-CD is about 19 wt.%, which allows it to stabilize in water. Most importantly, the high adsorption capability of the rGO-β-CD membrane indicates its outstanding separation performance for organic dyes and Cu (II) ions. The multi-mechanism of the Cu (II) ions removal in the rGO-β-CD membrane has been investigated systematically, the coordination effect with the carbonyl group, host-guest interaction, and the physical ion-sieving are the main reasons to improve the separation performance. This study provides a multi-mechanism membrane for the adsorption of organic dyes and Cu (II) ions in industrial wastewater, which has potential applications in water purification and desalination.

Conflict of interest

There are no conflicts to declare.

Supporting information

Additional details and figures on materials and methods are supplementary discussions.

References

[1] X. Yang, L. Liu, M. Zhang, W. Tan, G. Qiu, L. Zheng, Improved removal capacity of magnetite for Cr(VI) by electrochemical reduction, *Journal of Hazardous Materials*, 2019, **374**, 26-34, doi: 10.1016/j.jhazmat.2019.04.008.

[2] Y. Ding, S. Z. Shen, H. Sun, K. Sun, F. Liu, Synthesis of l-glutathione-capped-ZnSe quantum dots for the sensitive and selective determination of copper ion in aqueous solutions, *Sensors and Actuators B: Chemical*, 2014, **203**, 35-43, doi: 10.1016/j.snb.2014.06.054.

[3] M. Awual, A novel facial composite adsorbent for enhanced copper(II) detection and removal from wastewater, *Chemical Engineering Journal*, 2015, **266**, 368−375, doi: 10.1016/j.cej.2014.12.094.

[4] L. Cai, J. Sun, L. Cui, Y. Jiang, Z. Huang, Stabilization of heavy metals in piggery wastewater sludge through coagulation-hydrothermal reaction-pyrolysis process and sludge biochar for tylosin removal, *Journal of Cleaner Production*, 2020, **260**, 121165, doi: 10.1016/j.jclepro.2020.121165.

[5] M. Musielak, A. Gagor, B. Zawisza, E. Talik, R. Sitko, Graphene oxide/carbon nanotube membranes for highly efficient removal of metal ions from water, *ACS Applied Materials & Interfaces*, 2019, **11**, 28582-28590, doi: 10.1021/acsami.9b11214.

[6] F. Qin, Z. Fang, X. Qiu, Efficient Removal of Cu2+ in Water by Carboxymethylated Cellulose Nanofibrils: Performance and Mechanism, *Biomacromolecules*, 2019, **20**, 4466−4475, doi: 10.1021/acs.biomac.9b01198.

[7] P. Hadi, J. Barford, G. McKay, Toxic Heavy Metal Capture Using a Novel Electronic Waste-Based Material-Mechanism, Modeling and Comparison, *Environmental Science and Technology*, 2013, **47**, 8248−8255, doi: 10.1021/es4001664.

[8] X. Dong, Q. Ge, Metal ion-bridged forward osmosis membranes for efficient pharmaceutical wastewater reclamation, *ACS Applied Materials & Interfaces*, 2019, **11**, 37163-37171, doi: 10.1021/acsami.9b14162.

[9] M. L. Hidalgo, S. Hu, O. Marshall, A. Mishchenko, A. N. Grigorenko, R. A. W. Dryfe, B. Radha, I. V. Grigorieva, A. K. Geim, Sieving hydrogen isotopes through two-dimensional crystals, *Science*, 2016, **351**, 68-70, doi: 10.1126/science.aac9726.

[10] Y. Wang, W. Xie, H. Liu, H. Gu, Hyperelastic magnetic reduced graphene oxide three-dimensional framework with superb oil and organic solvent adsorption capability, *Advanced Composites and Hybrid Materials*, 2020, **3**, 473-484, doi: 10.1007/s42114-020-00191-z.

[11] K. Celebi, J. Buchheim, R. M. Wyss, A. Droudian, P. Gasser, I. Shorubalko, J.-I. Kye, C. Lee, H. G. Park, Ultimate permeation across atomically thin porous graphene, *Science*, 2014, **344**, 289-292, doi: 10.1126/science.1249097.

[12] H. W. Kim, H. W. Yoon, S.-M. Yoon, B. M. Yoo, B. K. Ahn, Y. H. Cho, H. J. Shin, H. Yang, U. Paik, S. Kwon, J.-Y. Choi, H. B. Park, Selective gas transport through few-layered graphene

and graphene oxide membranes, *Science*, 2013, **342**, 91-95, doi: 10.1126/science.1236098.
[13] L. Chen, G. Shi, J. Shen, B. Peng, B. Zhang, Y. Wang, F. Bian, J. Wang, D. Li, Z. Qian, G. Xu, G. Liu, J. Zeng, L. Zhang, Y. Yang, G. Zhou, M. Wu, W. Jin, J. Li, H. Fang, Ion sieving in graphene oxide membranes via cationic control of interlayer spacing, *Nature*, 2017, **550**, 380-383, doi: 10.1038/nature24044.
[14] N. I. Kovtyukhova, P. J. Ollivier, B. R. Martin, T. E. Mallouk, S. A. Chizhik, E. V. Buzaneva, A. D. Gorchinskiy, Layer-by-layer assembly of ultrathin composite films from micron-sized graphite oxide sheets and polycations, *Chemistry of Materials*, 1999, **11**, 771-778, doi: 10.1021/cm981085u.
[15] Y. Xu, H. Bai, G. Lu, C. Li, G. Shi, Flexible graphene films via the filtration of water-soluble noncovalent functionalized graphene sheets, *Journal of the American Chemical Society*, 2008, **130**, 5856-5857, doi: 10.1021/ja800745y.
[16] A. Z. M. Badruddoza, A. S. H. Tay, P. Y. Tan, K. Hidajat, M. S. Uddin, Carboxymethyl-β-cyclodextrin conjugated magnetic nanoparticles as nano-adsorbents for removal of copper ions: synthesis and adsorption studies, *Journal of Hazardous Materials*, 2011, **185**, 1177-1186, doi: 10.1016/j.jhazmat.2010.10.029.
[17] N.I. Kovtyukhova, P.J. Ollivier, B.R. Martin, Layer-by-Layer Assembly of Ultrathin Composite Films from Micron-Sized Graphite Oxide Sheets and Polycations, *Chemistry of Materials*, 1999, **11**, 771−778, doi: 10.1021/cm981085u.
[18] M. Cheng, L. Huang, Y. Wang, J. Tang, Y. Wang, Y. Zhao, G. Liu, Recent developments in graphene-based/nanometal composite filter membranes, *RSC Advances*, 2017, **7**, 47886−47897, doi: 10.1039/C7RA08098K.
[19] J. Yan, Z. Zhao, L. Pan, Growth and characterization of graphene by chemical reduction of graphene oxide in solution, *Physica Status Solidi (a)*, 2011, **208**, 2335-2338, doi: 10.1002/pssa.201084172.
[20] Y. Guo, S. Guo, J. Ren, Y. Zhai, S. Dong, E. Wang, Cyclodextrin functionalized graphene nanosheets with high supramolecular recognition capability: synthesis and Host−Guest inclusion for enhanced electrochemical performance, *ACS Nano*, 2010, **4**, 4001-4010, doi: 10.1021/nn100939n.
[21] A. Mondal, N. R. Jana, Fluorescent detection of cholesterol using β-cyclodextrin functionalized graphene, *Chemical Communications*, 2012, **48**, 7316, doi: 10.1039/c2cc33410k.
[22] P. K. Ang, S. Wang, Q. Bao, J. T. L. Thong, K. P. Loh, High-throughput synthesis of graphene by intercalation–exfoliation of graphite oxide and study of ionic screening in graphene transistor, *ACS Nano*, 2009, **3**, 3587-3594, doi: 10.1021/nn901111s.
[23] D. Li, M. B. Müller, S. Gilje, R. B. Kaner, G. G. Wallace, Processable aqueous dispersions of graphene nanosheets, *Nature Nanotechnology*, 2008, **3**, 101-105, doi: 10.1038/nnano.2007.451.
[24] H. Bai, Y. Xu, L. Zhao, C. Li, G. Shi, Non-covalent functionalization of graphene sheets by sulfonated polyaniline, *Chemical Communications*, 2009, **1667**, doi: 10.1039/b821805f.
[25] Y. Xu, H. Bai, G. Lu, C. Li, G. Shi, Flexible graphene films via the filtration of water-soluble noncovalent functionalized graphene sheets, *Journal of the American Chemical Society*, 2008, **130**, 5856-5857, doi: 10.1021/ja800745y.
[26] Y. Xing, L. Li, C. C. Chusuei, R. V. Hull, Sonochemical oxidation of multiwalled carbon nanotubes, *Langmuir*, 2005, **21**, 4185-4190, doi: 10.1021/la047268e.
[27] L. A. Langley, D. E. Villanueva, D. H. Fairbrother, Quantification of surface oxides on carbonaceous materials, *Chemistry of Materials*, 2006, **18**, 169-178, doi: 10.1021/cm051462k.
[28] K. Kimura, G. Amy, J. E. Drewes, T. Heberer, T.-U. Kim, Y. Watanabe, Rejection of organic micropollutants (disinfection by-products, endocrine disrupting compounds, and pharmaceutically active compounds) by NF/RO membranes, *Journal of Membrane Science*, 2003, **227**, 113-121, doi: 10.1016/j.memsci.2003.09.005.
[29] Z. Lü, F. Hu, H. Li, X. Zhang, S. Yu, M. Liu, C. Gao, Composite nanofiltration membrane with asymmetric selective separation layer for enhanced separation efficiency to anionic dye aqueous solution, *Journal of Hazardous Materials*, 2019, **368**, 436-443, doi: 10.1016/j.jhazmat.2019.01.086.
[30] P. Tan, Y. Hu, Improved synthesis of graphene/β-cyclodextrin composite for highly efficient dye adsorption and removal, *Journal of Molecular Liquids*, 2017, **242**, 181−189, doi: 10.1016/j.molliq.2017.07.010.
[31] R. K. Joshi, P. Carbone, F. C. Wang, V. G. Kravets, Y. Su, I. V. Grigorieva, H. A. Wu, A. K. Geim, R. R. Nair, Precise and ultrafast molecular sieving through graphene oxide membranes, *Science*, 2014, **343**, 752-754, doi: 10.1126/science.1245711.
[32] P. Sun, K. Wang, H. Zhu, Recent developments in graphene-based membranes: structure, mass-transport mechanism and potential applications, *Advanced Materials*, 2016, **28**, 2287-2310, doi: 10.1002/adma.201502595.
[33] T.A. Saleh, Simultaneous adsorptive desulfurization of diesel fuel over bimetallic nanoparticles loaded on activated carbon, *Journal of Cleaner Production*, 2018, **172**, 2123−2132, doi: 10.1016/j.jclepro.2017.11.208.